Investigation of Cavitation Phenomena in a “High-Power” Piezohydraulic Pump: A Computational Fluid Dynamics (CFD) Approach

Journal of Physics: Conference Series **2893** (2024) 012060 doi:10.1088/1742-6596/2893/1/012060

Investigation of Cavitation Phenomena in a "High-Power" Piezohydraulic Pump: A Computational Fluid Dynamics (CFD) Approach

Francesco Sciatti[1*], Vincenzo Di Domenico[1], Paolo Tamburrano[1], Nathan Sell[2], Andrew R. Plummer[2], Elia Distaso[1], Giovanni Caramia[1] and Riccardo Amirante[1]

[1] Department of Mechanics, Mathematics and Management (DMMM), Polytechnic University of Bari, 70121 Bari, Italy;
[2] Centre for Power Transmission and Motion control (PTMC), University of Bath, Bath BA2 7AY, UK.

[*]Corresponding author: francesco.sciatti@poliba.it

Abstract. Piezoelectric pumps, known as piezopumps, are highly versatile devices with applications in various fields due to their precise flow control, compact design, lack of magnetic interference, and low noise. These pumps are classified based on the number of pumping chambers, valve configuration, and driving power source mechanism. In fields requiring consistent flow rates and back pressures, particularly in fluid power applications, piezopumps employing a piezostack actuator as their power driving source are actively researched. This kind of piezopumps, also known as piezohydraulic pumps, operate using a piezostack actuator to drive a piston for fluid delivery, along with reed valves controlling fluid flow at the inlet and outlet of the pump chamber. The high operating frequency range of the piezostack actuator and reed valves, exceeding 1 kHz, allows piezohydraulic pumps to achieve significant flow rates despite the stack's limited displacement. This enhances their performance without the need for increased size or power input. However, this also increases the risk of cavitation, which could lead to damage, reduced efficiency, and higher noise levels. Therefore, the purpose of this paper is to expand on previous research by using the CFD software Ansys Fluent to further investigate cavitation phenomena in a piezohydraulic pump developed at the University of Bath. In particular, the study focuses on simulating various oil flow scenarios through the pump with a fixed inlet pressure of 20 bar, while varying the opening of the inlet reed valve from the minimum (0.1 mm) to maximum (0.7 mm) value, as well as adjusting the pump chamber pressure.

1. Introduction

Conventional hydraulic pumps, both dynamic pumps and positive displacement pumps, are machines designed to boost the energy of liquid as it flows through them. Specifically, these devices convert the mechanical energy from a prime mover, such as an electric motor, into hydraulic fluid power [1], [2]. While the design and manufacturing processes for these pumps are well-established, advancements in fields like chemistry, biomedicine, aerospace, robotics, and

liquid cooling have increased the demand for pumps that are more reliable, compact, simple in design, capable of precise flow control, and operate quietly. Conventional hydraulic pumps struggle to meet these demands due to inherent structural limitations [3], [4], [5], [6].

One promising solution to meet the previous stringent requirements and realize precision fluid pumps is the use of piezoelectric actuators. Due to their large output force, rapid dynamic response, high reliability, simple structure and light weigh, piezoelectric actuators have been successfully used in fluid power applications [7], [8], [9]. Specifically, these smart actuators have been employed to address common issues associated with conventional proportional and servovalves, including direct drive and two-stage servovalves. This has led to the creation of innovative and miniaturized valves, known as piezoelectric valves or piezovalves [10], [11], [12]. Miniaturization is particularly critical in medical and aerospace applications, where these valves are essential for controlling gas flow in lung ventilators for intensive care units and managing fuel supply in aircraft fuel systems [13], [14], [15], [16], [17].

Piezoelectric pumps, or piezopumps, utilize the inverse piezoelectric effect of piezoelectric materials to convert electrical energy into mechanical energy, which is then used to pressurize and move fluids. Piezopumps can incorporate one or multiple pumping chambers and can function with or without valves, using either piezomembrane or piezostack actuators as driving power source for fluid delivery [18]. These components enable piezopumps to address issues such as leakage, wear, and fatigue damage caused by moving parts, while also reducing energy loss compared to conventional hydraulic pumps [18], [19].

The performance of piezopumps can vary based on factors like the driving voltage, driving frequency, and specific configuration [18]. However, despite advancements in technology, achieving output flow rates exceeding 1 L/min and back pressures greater than 1 bar remains uncommon, with only a limited number of examples reported in the literature [20], [21], [22].

In fluid power applications, where high flow rates and back pressures are required, piezostack actuators are preferred over piezomembrane actuators as the driving power source mechanism, especially when combined with a valve-based configuration [23], [24], [25]. Additionally, while multiple pumping chambers can potentially enhance the performance metrics, this design also introduces complexity and higher costs [26], [27], [28]. Therefore, a single pumping chamber is typically favoured for its simplicity and cost-effectiveness [29]. Piezopumps that use piezostack actuators as their driving power source are also known as piezohydraulic pumps.

In a conventional piezohydraulic pump, a piezostack actuator drives a piston, and a pair of check valves (inlet and outlet) control the fluid flow into and out of the pumping chamber. The working cycle of such a piezopump, illustrated in Figure 1, consists of four stages:

A) Compression Stage: Both inlet and outlet check valves (3 – 4) are closed. When the voltage signal is applied to the piezostack actuator (1), it expands, compressing the fluid by means of the piston (2), thereby increasing the pressure in the pumping chamber (5);
B) Delivery Stage: When the pumping chamber pressure matches the outlet pressure, the outlet check valve opens, allowing fluid to flow out.
C) Expansion Stage: Removing the voltage signal causes the piezostack actuator to contract, reducing the pumping chamber pressure to the inlet level.
D) Intake Stage: The inlet check valve opens when the inlet pressure and pumping chamber pressure equalize, letting fluid back into the pumping chamber.

Thanks to the high operating frequency of piezoelectric actuators and reed valves (a type of passive check valve made from flexible materials), which can exceed 1 kHz [30], piezopumps can

achieve high flow rates despite the limited displacement of the piezostack actuator. Increasing the driving frequency is a simple and effective way to enhance the performance of piezopumps [31]. However, at high driving frequencies, piezopumps are prone to severe cavitation [32], which can lead to component damage, reduced efficiency, vibrations, and noise [33].

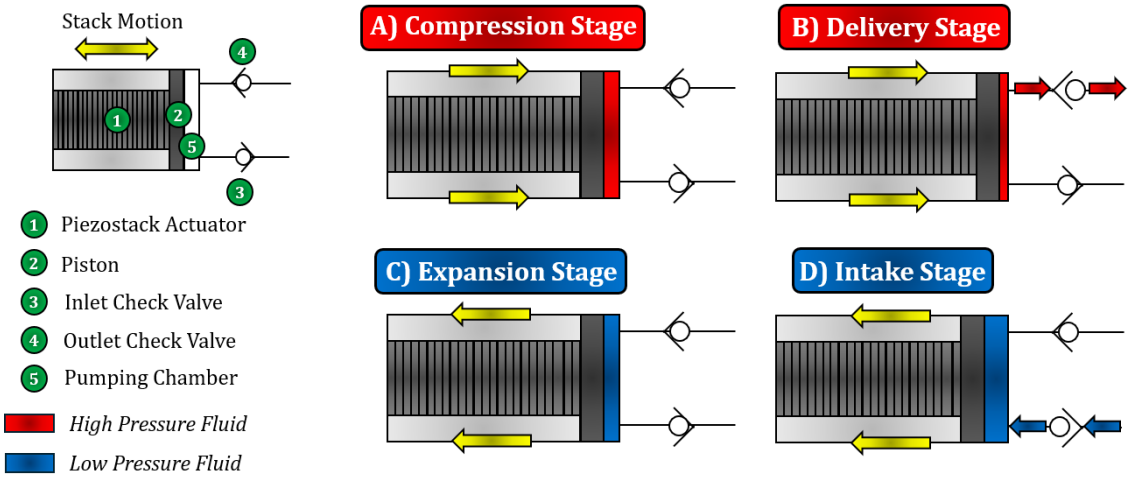

Figure 1. The four-stage working cycle of a conventional piezohydraulic pump.

Cavitation, which involves the formation, growth, and implosive collapse of vapour bubbles under high-pressure conditions, significantly limits the performance of piezopumps working at high flow rates [34]. Zhang et al. found that during the intake stage, as the pumping chamber volume increases and pressure decreases, dissolved gas escapes from the liquid, leading to cavitation [32]. He et al. explored the negative impacts of cavitation on piezopumps, noting that it reduces the bulk modulus of the working fluid, thereby severely decreasing pump efficiency [35]. In efforts to mitigate cavitation, Pecar et al. utilized a sinusoidal excitation signal waveform, which, despite resulting in lower output flow rates, effectively reduced the risk of cavitation compared to square-wave excitation [36], [37].

In this scenario, this paper continues a numerical investigation into cavitation potential in a specific piezohydraulic pump developed at the University of Bath, as initiated in [38], using the CFD software Ansys Fluent. The study specifically focuses on simulating various oil flow scenarios through the pump under a fixed inlet pressure of 20 bar. The investigation varies the opening of the inlet reed valve from its minimum (0.1 mm) to maximum (0.7 mm) values, while also adjusting the pumping chamber pressure.

The architecture, including exploration of all components of the piezohydraulic pump under investigation, is presented first. Then, the test rig used to evaluate the pump prototype along with the corresponding experimental results, which highlight cavitation issues, are provided. Next, the 3D CAD model of the pump and the three approximations used to obtain a simplified 2D domain, including its corresponding computational grid using unstructured tetrahedral meshes, are illustrated. Finally, the numerical results of the computational fluid dynamic (CFD) analysis are examined in order to evaluate potential situations that may lead to cavitation. Specifically, the simulations will be conducted by exploring all possible degrees of opening of the inlet reed valve and different pumping chamber pressure values.

2. Piezohydraulic Pump Prototype

The architecture of the piezohydraulic pump prototype developed at the University of Bath [22] is now fully examined. The design makes use of a ring stack actuator from PI Ceramic, model PICA P025.50H, as its driving force for fluid delivery. This actuator provides a blocking force of 9.6 kN and has a maximum extension (or free stroke) of 80 µm. Detailed specifications are available in Table 1 [39].

Table 1. PICA P025.50H ring stack actuator: specifications [39].

Parameter	Value	Unit
Cross-Sectional Area	2.89	cm^2
Outer Diameter	25	mm
Inner Diameter	16	mm
Length	66	mm
Maximum Voltage	1000	V
Free Stroke	80	μm
Blocking Force	9.6	kN
Capacitance	1.2	μF
Natural Frequency	17	kHz

The ring stack actuator drives a 26.7 mm diameter piston, forming the core of the piezohydraulic pump. Figure 2 presents a longitudinal section view of the ring stack actuator and piston assembly, with a detailed bill of materials available in Table 2.

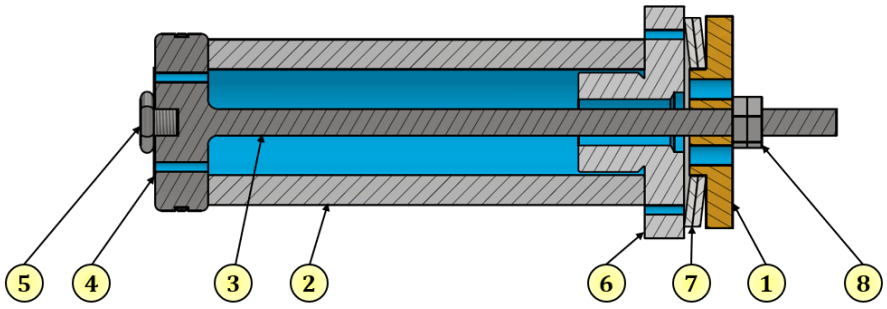

Figure 2. Longitudinal section view of the ring stack actuator – piston assembly, with blue indicating the low-pressure fluid pathway.

The choice of a ring stack as piezoelectric actuator offers several advantages:

- Compact Design: The inlet flow, entering through the eight orifices of the inlet plate (1), passes through the cavity of the ring stack actuator (2) and enters the pumping chamber via the

twelve orifices of the piston (3). This allows the disc-style inlet reed valve (4) to be positioned on the left end face of the piston with a valve screw (5), resulting in a more compact design;

- Preloading Mechanism: The piston rod, passing through the hole of the ring stack actuator, clamps and preloads the stack using the piston clamp (6), Belleville washers (7), and bolts (8). This configuration provides a convenient way to preload the stack;
- Enhanced Lifetime: Pre-compression is necessary because piezostack actuators cannot handle large pulling forces. Applying a preload helps prevent damage and significantly extends the actuator's lifetime, with optimal preload values ranging from 20 to 50 percent of the blocking force [39], [40].

Table 2. Bill of materials of the ring stack actuator – piston assembly.

Part Number	Item
1	Inlet Plate
2	Ring Stack Actuator
3	Piston
4	Inlet Reed Valve
5	Valve Screw
6	Piston Clamp
7	Belleville Washers
8	Bolts

The pumping chamber, with a height of only 1 mm, is confined between the piston and the valve plate. The latter has a similar arrangement to the piston, including twelve orifices and an outlet reed valve positioned on its left end face with another valve screw. This setup allows the extension and retraction of the ring stack actuator to control the opening and closing of the inlet and outlet reed valves. Depending on the internal pressure, these valves allow fluid to flow out of the pumping chamber during the delivery stage and into the pumping chamber during the intake stage.

Figure 3(a) provides a longitudinal section view of the entire pump, showing the position of the 0.2 mm thick disc-style reed valves. Figure 3(b) displays the valve disc itself with the corresponding valve screw. Finally, Figure 3(c) shows the prototype of the assembled piezopump tested at the University of Bath [22].

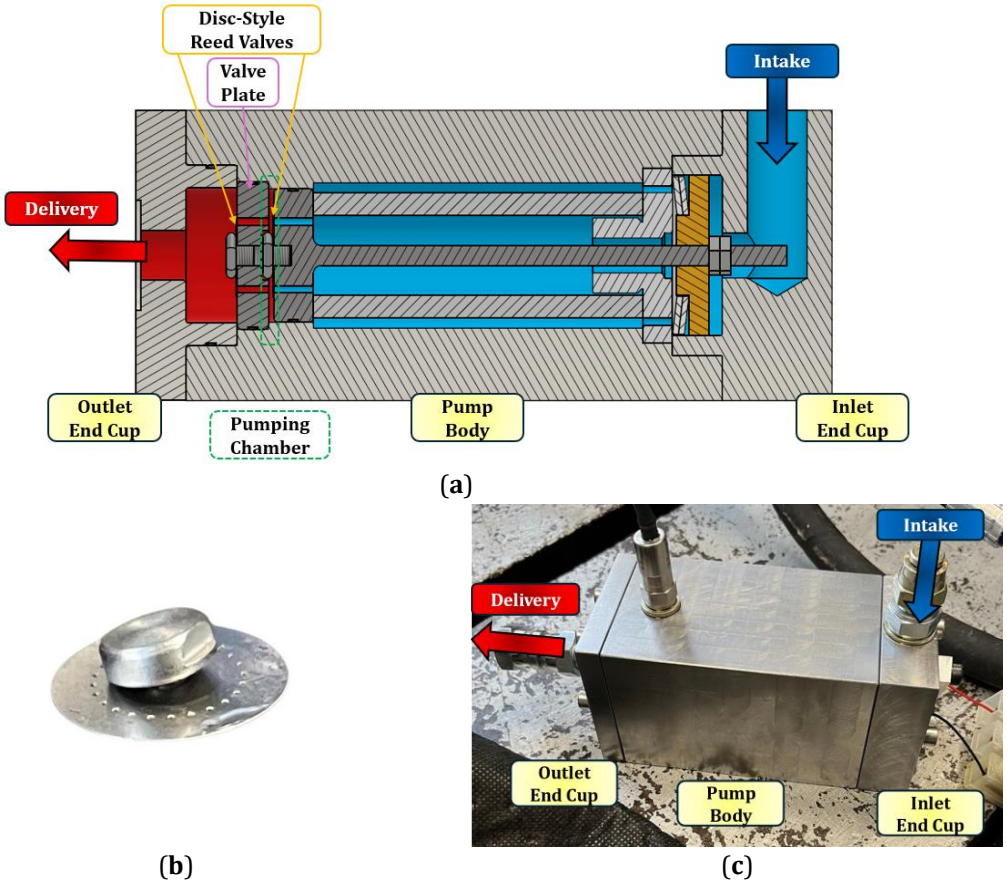

Figure 3. Piezohydraulic pump developed at the University of Bath [22]: (**a**) Longitudinal section view of the entire pump; (**b**) Thick disc-style reed valve with corresponding valve screw; (**c**) Assembled Pump Prototype.

3. Test Rig, Experimental Results and Cavitation Issues

To assess the performance of the piezohydraulic pump, a prototype was tested in a simple loading system [22], depicted schematically in Figure 4(a) with detailed components listed in Table 3. Figure 4(b) provides a photo of the test setup.

In the test setup, oil from the pump flowed through a 3-meter-long pipe with a 6 mm diameter. A direct drive servovalve at the pipe's end allowed for varying load pressures. To safeguard against potential over-pressure situations and damage, a pressure relief valve set to open at 200 bar was installed. The pump maintained a constant inlet pressure of 20 bar to enhance oil stiffness and prevent cavitation.

During testing at 950 V driving voltage and 1250 Hz frequency, with a 15 bar load pressure, the pressure in the pumping chamber dropped to nearly 0 bar, suggesting possible cavitation due to high pressure drop across the inlet reed valve [22]. Despite this issue, the pump demonstrated a mean flow rate of 1.05 L/min and generated approximately 30 W of hydraulic power. For this reason, the authors termed this kind of piezopump a "high-power" piezohydraulic pump [22], as piezopumps achieving this output power are uncommon in the literature, as previously discussed in the Introduction.

Due to the difficulty in visually confirming cavitation within the piezohydraulic pump, the occurrence of cavitation needs to be studied further through a detailed computational fluid dynamics (CFD) analysis. Therefore, the next section will present a CFD analysis conducted using Ansys Fluent software to assess potential cavitation scenarios.

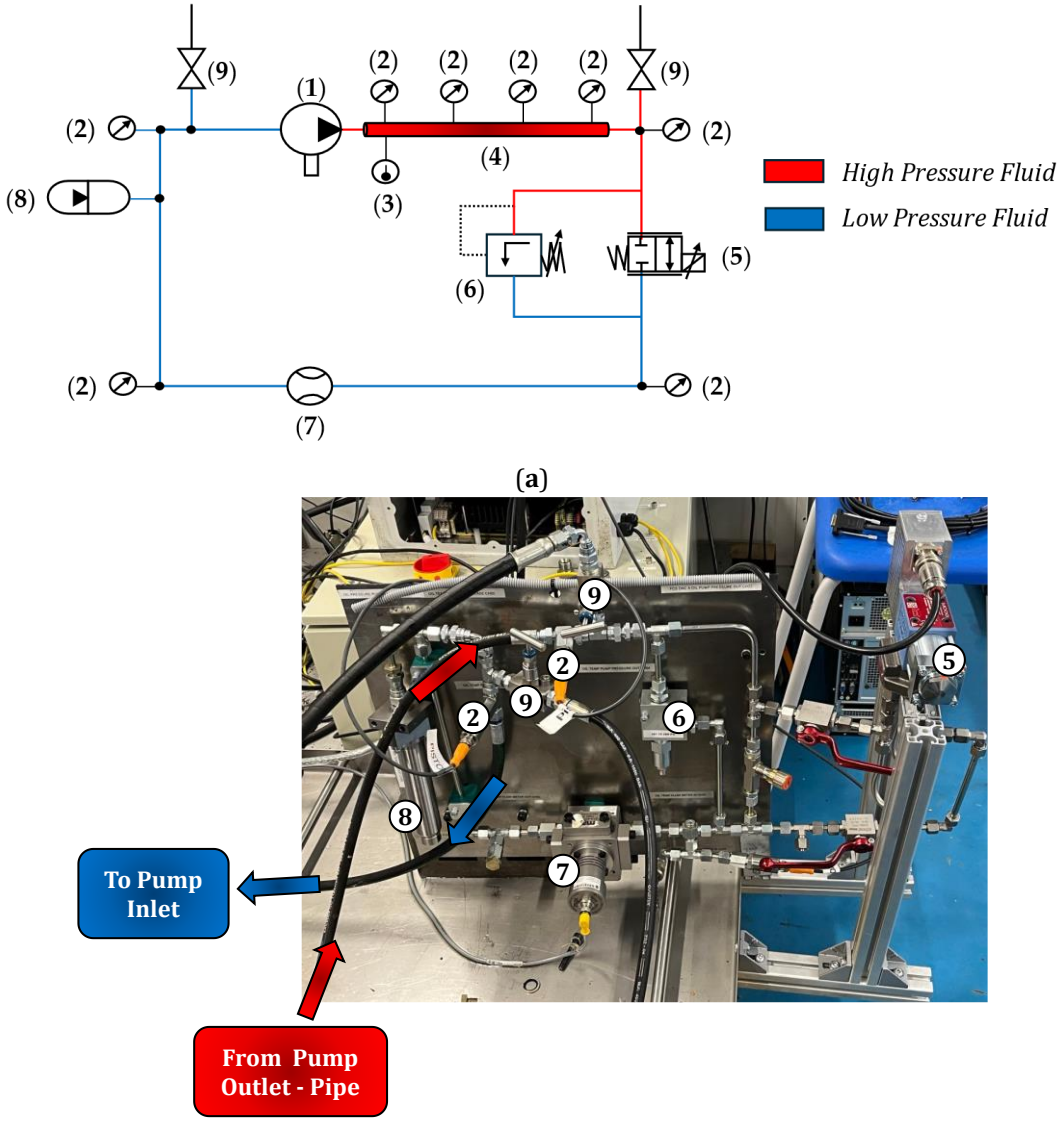

Figure 4. Test rig for evaluating pump performance: (**a**) Schematic circuit; (**b**) Photograph of the setup.

Table 3. Test rig components.

Number	Component
1	Piezohydraulic Pump
2	Pressure Sensor
3	Temperature Sensor
4	Pipe
5	Direct Drive Servovalve
6	Pressure Relief Valve
7	Flow Sensor
8	Accumulator
9	Needle Valve

4. Computational Fluid Dynamic Analysis

4.1 Simplified Model for Cavitation Investigation

The computational fluid dynamics (CFD) analysis of the piezohydraulic pump developed at the University of Bath began with the creation of a 3D model using Autodesk Inventor Professional. This 3D model is shown in Figure 5(a).

To better understand the operating conditions that might lead to cavitation during the intake stage, particularly focusing on the different openings of the inlet reed valve, the 3D model was simplified into a 2D model through three key approximations:

1. Creating a Simplified 3D Domain: Two cutting planes were marked on the 3D model to create a simplified 3D domain, as shown in Figure 5(b). This domain includes the oil within the inner part of the ring stack, the twelve piston orifices, and part of the pumping chamber, as depicted in Figure 5(c). The oil between the ring stack actuator and the pump body was omitted because it is not influential in analysing cavitation.
2. Considering Geometry Axial Symmetry: Due to the axial symmetry of the pump's geometry, only a slice of this simplified 3D domain was examined. This slice contains the oil flowing into one of the twelve piston orifices, highlighted in green in Figure 5(c).
3. Focusing on the Mid-Plane Section: The analysis focused only on the mid-plane section of this slice to investigate potential cavitation scenarios, leading to the development of the 2D simplified model system of the piezohydraulic pump, illustrated in Figure 5(d).

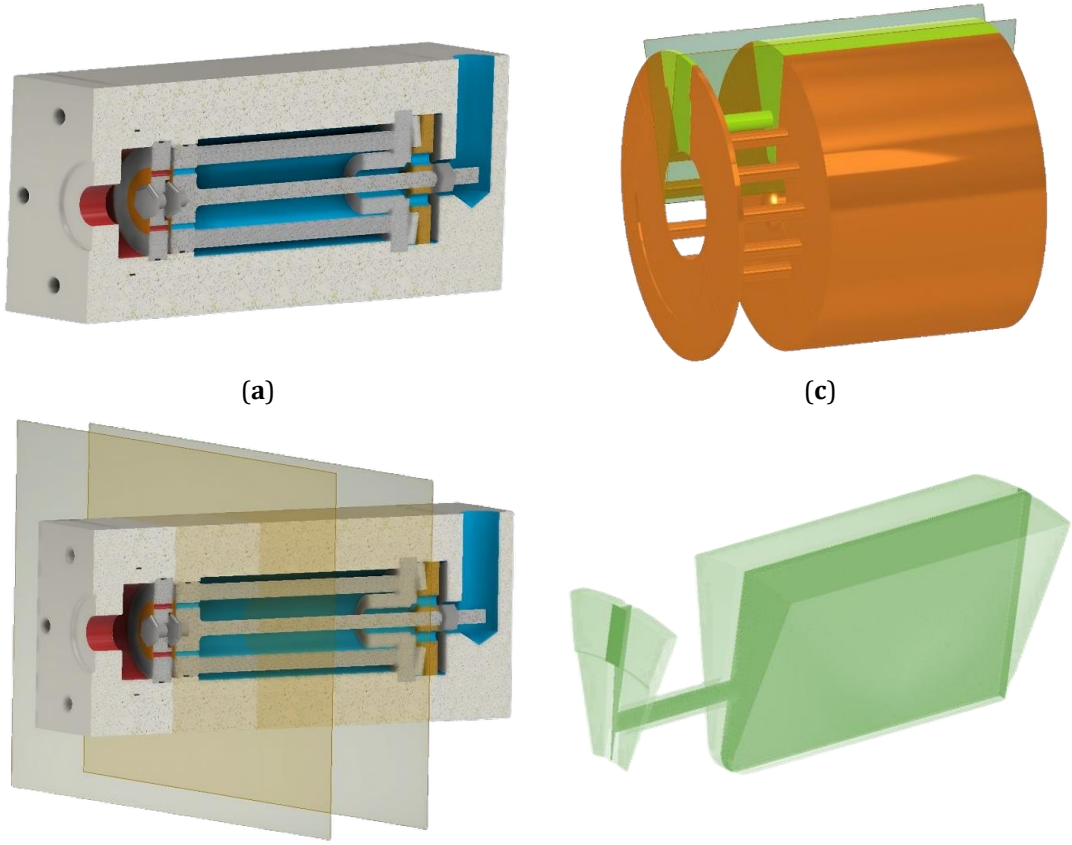

Figure 5. Piezohydraulic pump developed at the University of Bath [22]: (**a**) 3D model created using Autodesk Inventor Professional; (**b**) Two cutting planes used to simplify the 3D domain; (**c**) Oil included in the simplified 3D domain, with the slice due to axial symmetry highlighted in green; (**d**) 2D model system resulting from the mid-plane section of the slice.

4.2 Computational Mesh

The 2D model system, based on previous considerations, was discretized using Cadence Fidelity Pointwise. Unstructured meshes, composed of triangle elements with explicit connectivity, were employed in this analysis for their flexibility and automation in the generation process [40]. The grid was created for all possible openings of the inlet reed valve, ranging from 0.1 mm (minimum value) to 0.7 mm (maximum value) in 0.1 mm increments.

For non-restricted parts of the pump, the mesh setup used fewer than 25 points, resulting in large interval sizes from 0.1 mm to 0.9 mm. In contrast, for the edges of the piston orifice and the inlet reed valve, more than 1,000 points were used, creating very small interval sizes from 0.0025 mm to 0.01 mm. This detailed approach aimed to identify pressure and velocity gradients and flow swirls to predict potential cavitation during the intake stage, when oil flows through the small passage uncovered by the inlet reed valve opening.

After discretizing all edges, the entire flow domain was meshed for the seven different cases corresponding to the seven different openings of the inlet reed valve. Figure 6 provides images of three of the seven computational meshes of the 2D pump model system, specifically for inlet reed valve openings of 0.1 mm, 0.4 mm, and 0.7 mm. It is important to note that the seven

computational meshes each use fewer than 57,000 total cells, resulting in a relatively low computational cost for obtaining the CFD simulations.

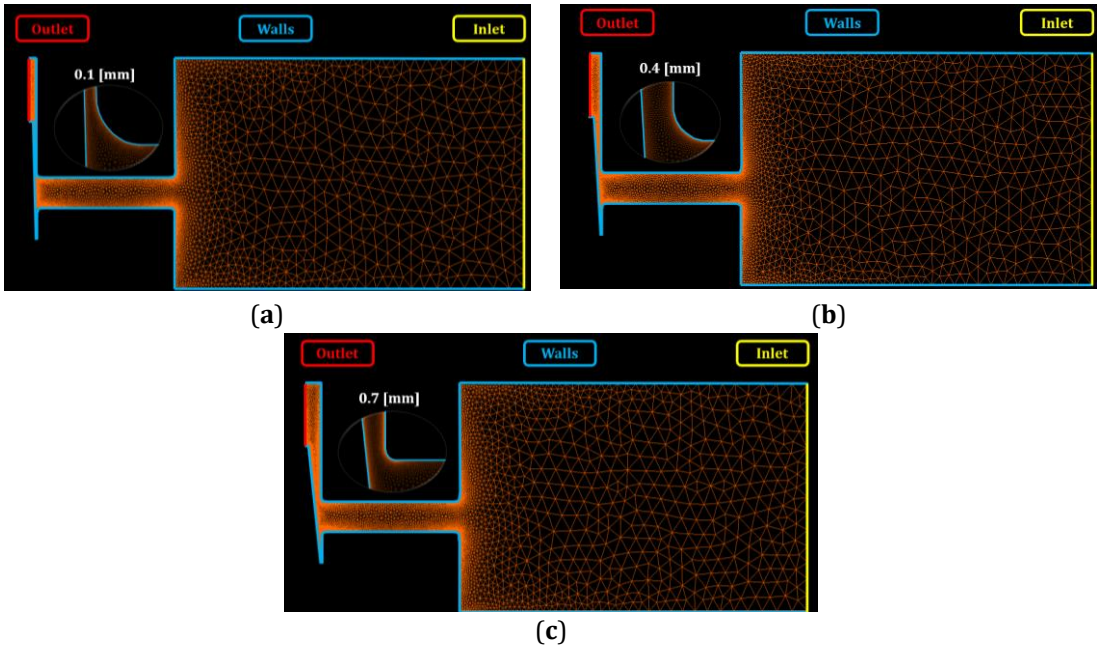

Figure 6. Computational mesh of the 2D pump model system for three different openings of the inlet reed valve: (**a**) 0.1 [mm]; (**b**) 0.4 [mm]; (**c**) 0.7 [mm].

Finally, Table 4 provides a detailed description of the boundary conditions set before exporting the seven computational grids.

Table 4. Boundary Conditions.

Zone/Line	Boundary Condition	Description
Inlet	Pressure Inlet (p_{in})	Fixed Pressure at the pump inlet
Outlet	Pressure Outlet (p_{cham})	Pressure value set in the pumping chamber during intake stage
Walls	—	Lines in the 2D meshed model system defining the walls
Oil Zone	—	Area bounded by the inlet, outlet, and walls.

4.3 Governing Equations

The seven computational grids were imported into Ansys Fluent for CFD simulations. Table 5 below summarizes all the conditions that were configured in Ansys Fluent for obtaining these simulations. The SIMPLE algorithm was selected for solving the problem due to its suitability for the involved physics. Cavitation was simulated using the Schnerr and Sauer equations, as well documented in [41]. Turbulence prediction utilized the SST k-ω method, due to its accuracy and a

low margin of error on simulation results [42]. Initially, turbulence equations for k and ω, as well as momentum equations, were solved using first-order upwind discretization, followed by second-order upwind discretization to stabilize the simulation. Pressure interpolation employed the PRESTO! scheme, which is considered a good choice for flows with steep pressure gradients [43]. The table also shows the values set for the density and viscosity of the liquid oil and vapour oil, as well as the vapour pressure. Regarding termination criteria, simulations were stopped when the mass flow rate maintained its third significant digit unchanged.

Table 5. Setting employed in Ansys Fluent for simulations.

Equation	**Multiphase (Mixture) Model**
Solver	SIMPLE
Turbulence Model	SST k-ω
Cavitation Model	Schnerr and Sauer
Discretization of Pressure Equation	PRESTO!
Discretization of Volume Fraction	First order upwind
Discretization of Momen. and Turbulence	Second order upwind
Under-relaxation of Pressure	0.3
Under-relaxation of Volume Fraction	0.5
Under-relaxation of Momentum	0.7
Under-relaxation of Turbulence Quantities	0.8
Inlet Pressure (p_{in})	20 bar absolute
Chamber Pressure (p_{cham})	Variable
Density and Viscosity Liquid-Oil	866 kg/m^3; 0.027 kg/(m·s)
Density and Viscosity Vapour-Oil	4 kg/m^3; $3 \cdot 10^{-06}$ kg/(m·s)
Vapour Pressure	10 Pa
Bubble Number Density	Default
Termination Criterion	Convergence in Mass-Flow Rate (third digit)

5. CFD Simulation Results

In this 2D simplified analysis, simulations aimed to assess potential scenarios that could trigger cavitation by considering a fixed inlet pump pressure of p_{in} =20 bar. The simulations varied the openings of the inlet reed valve (v_{opn}) from 0.1 mm (minimum value) to 0.7 mm (maximum value) in increments of 0.1 mm. Additionally, different plausible values of the pumping chamber pressure (p_{cham}) during the intake stage, derived from experimental pump results, were considered. Specifically, for each opening degree of the inlet reed valve, the simulations started by setting a very low pumping chamber pressure (0.5 bar) and increased it by 0.5 bar increments until a specific pumping pressure value no longer caused additional cavitation. Therefore, several steady-state scenarios regarding the intake stage were analysed. It is also important to note that these simulations were conducted with a relative pressure of 1.01 bar in mind.

Figure 7 and Figure 8 display the CFD simulation results depicting the velocity contour, pressure contour, and volume fraction of the vapour oil phase for an inlet reed valve opening v_{opn}= 0.4 mm and two different pumping chamber pressures, specifically p_{cham} = 2 bar and p_{cham} = 5 bar, respectively. Upon analysing Figure 7 and Figure 8, it becomes evident that the pumping chamber pressure significantly influences the velocity and pressure fields within the 2D oil domain for a fixed inlet reed valve opening. Specifically, the lower pumping chamber pressure (p_{cham} = 2 bar) caused a higher pressure drop across the inlet reed valve, resulting in a greater increase in average oil velocity near the restriction area, with a maximum computed value of 69.7 m/s. Consequently, local pressure values dropped below the vapour pressure, triggering vapour oil phase formation and subsequent cavitation. Additionally, it is important to note that both pumping chamber pressures considered (p_{cham} = 2 bar and p_{cham} = 5 bar) led to vapour oil phase formation and then cavitation; however, the higher pumping chamber pressure (p_{cham} = 5 bar) resulted in a reduced area of the vapour oil phase.

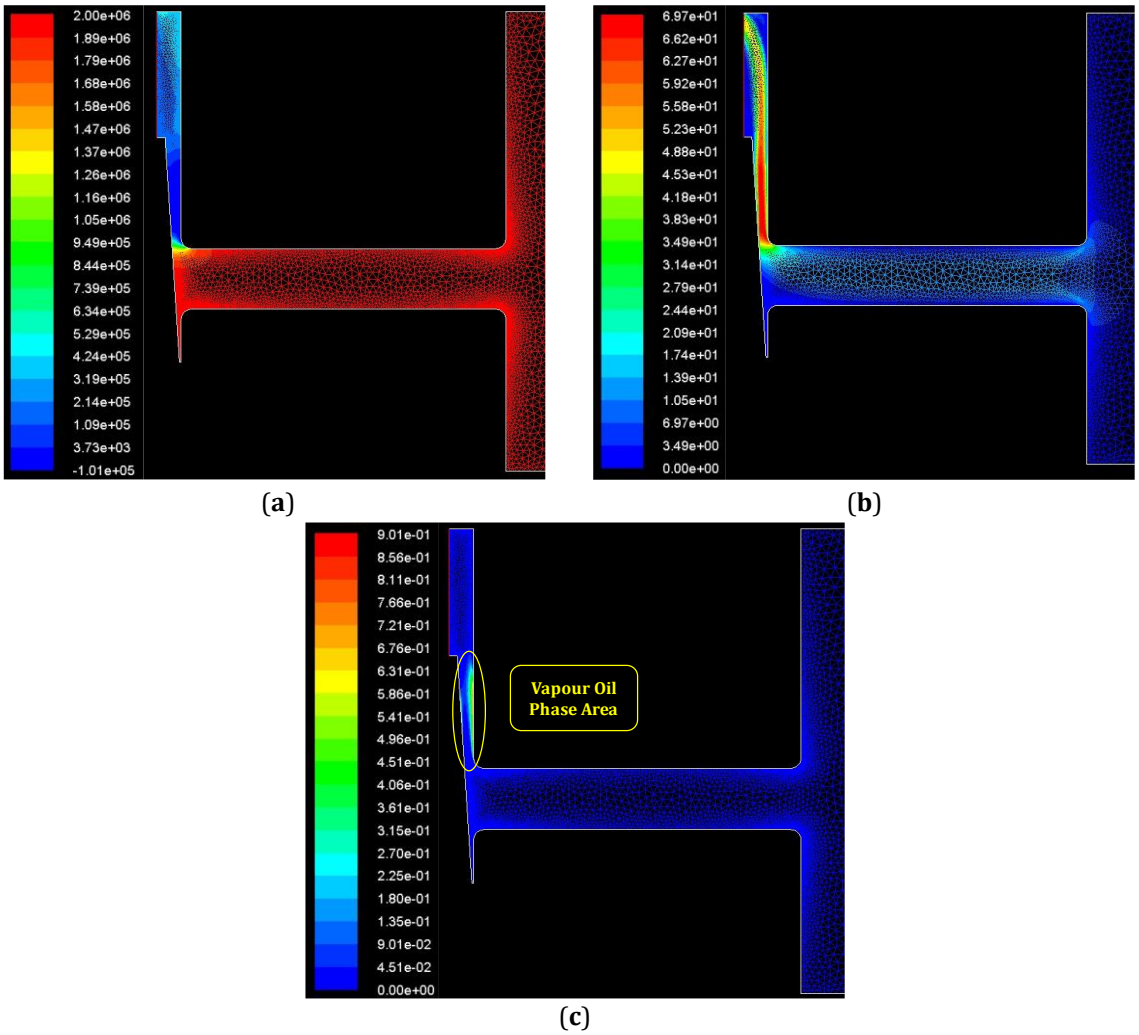

Figure 7. CFD simulation results considering p_{in} =20 bar, v_{opn} =0.4 mm and p_{cham} =2 bar: (**a**) Pressure Contour [Pa]; (**b**) Velocity Contour [m/s]; (**c**) Volume fraction of vapour oil phase [-].

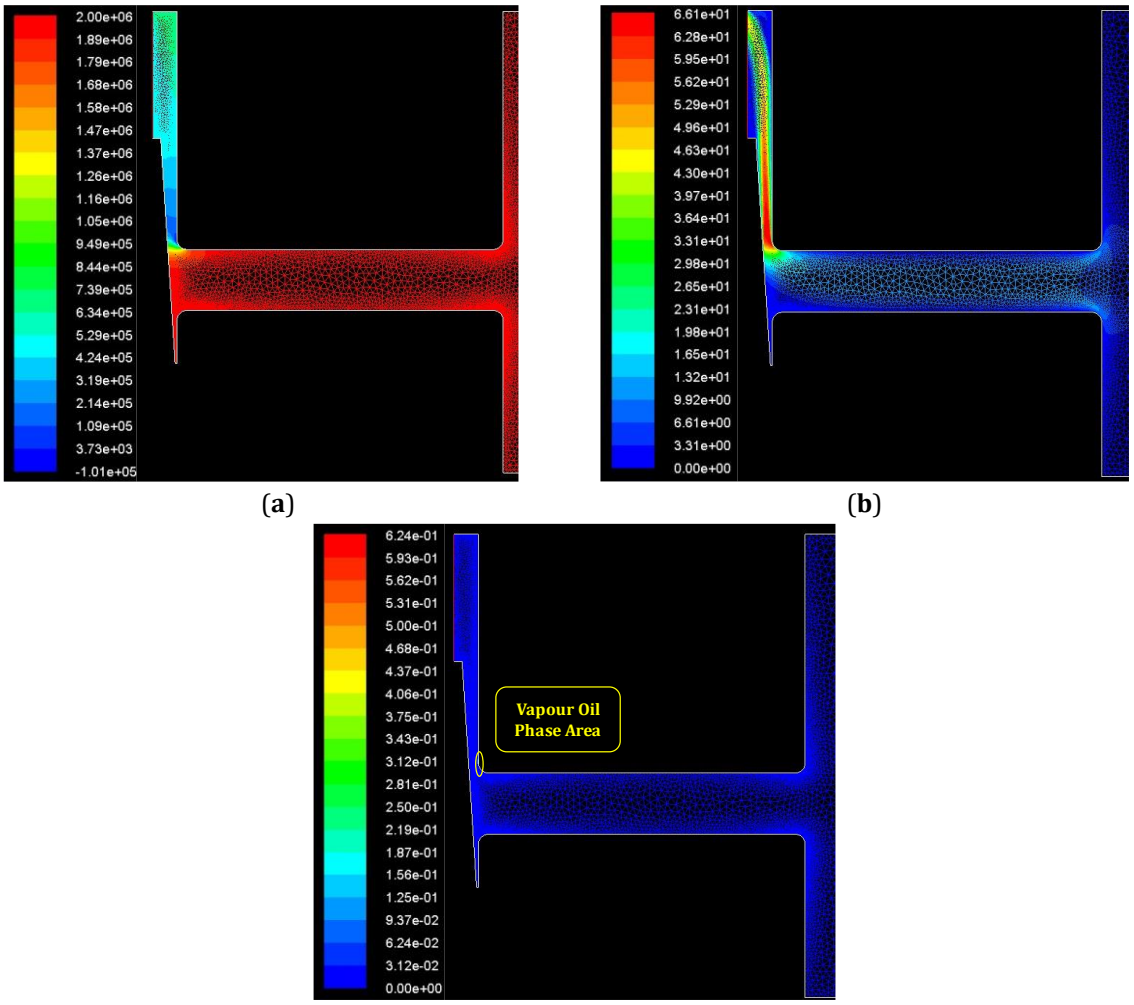

Figure 8. CFD simulation results considering p_{in} =20 bar, v_{opn} =0.4 mm and p_{cham} = 5 bar: (**a**) Pressure Contour [Pa]; (**b**) Velocity Contour [m/s]; (**c**) Volume fraction of vapour oil phase [-].

To analyse the effect of varying both the inlet reed valve opening v_{opn} and chamber pressure p_{cham}, Figure 9 and Figure 10 illustrates that as the opening of the inlet reed valve increases and the chamber pressure decreases, both the area of the vapour oil phase and the volume fraction of vapour oil also increase. This trend potentially leads to higher occurrences of cavitation because the decreasing chamber pressure, combined with an increased inlet reed valve opening, causes an increase in average velocity near the restricted area, leading to lower local pressure values and triggering cavitation, as shown in Figure 11.

The semi-logarithmic plots in Figures 9(b) and 10(b) provide a better understanding of the extremely low values of the vapor oil phase area and volume vapor oil fraction that can be achieved for specific input conditions (v_{opn} and p_{cham}).

Additionally, Figures 9, 10, and 11 show that despite the minimum value of pumping chamber pressure considered (p_{cham} = 0.5 bar), very low openings of the inlet reed valve (v_{opn} = 0.1 mm and v_{opn} = 0.2 mm), do not trigger vapor phase formation since the maximum average oil velocity near the restricted area in both cases is lower than 60 m/s, which can be considered a threshold value for triggering cavitation.

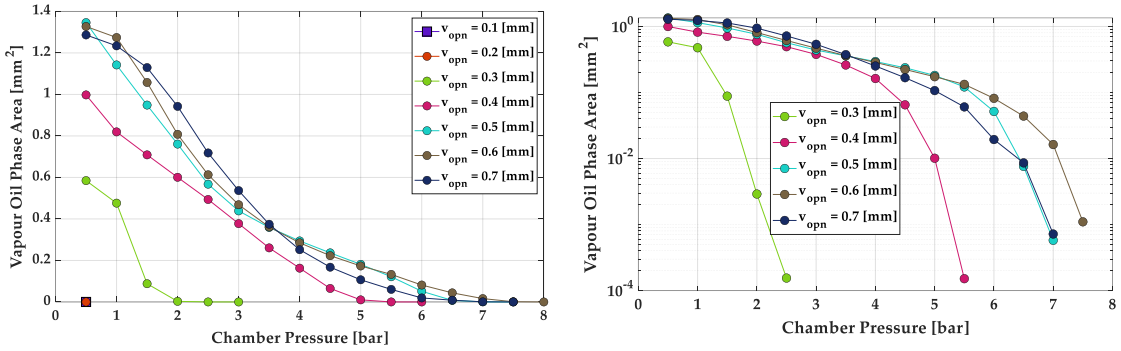

(**a**) (**b**)

Figure 9. Vapour oil phase area [mm²] with p_{in} =20 bar, varying v_{opn} from 0.1 mm to 0.7 mm (increments of 0.1 mm) and p_{cham} (increment of 0.5 bar starting from 0.5 bar): (**a**) Normal Plot; (**b**) Semi-logarithmic Plot.

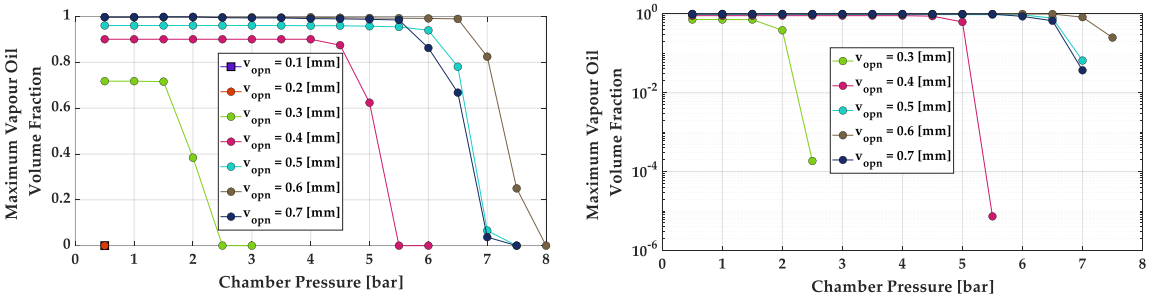

(**a**) (**b**)

Figure 10. Vapour oil volume fraction with p_{in} =20 bar, varying v_{opn} from 0.1 mm to 0.7 mm (increments of 0.1 mm) and p_{cham} (increment of 0.5 bar starting from 0.5 bar): (**a**) Normal Plot; (**b**) Semi-logarithmic Plot.

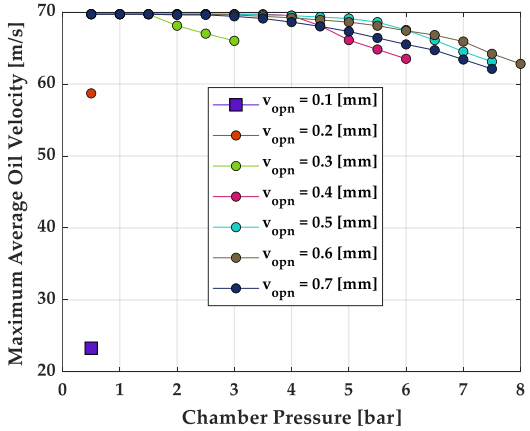

Figure 11. Maximum average oil velocity near the restricted area [m/s] with p_{in} =20 bar, varying v_{opn} from 0.1 mm to 0.7 mm (increments of 0.1 mm) and p_{cham} (increment of 0.5 bar starting from 0.5 bar).

Finally, Figure 12 presents a heatmap illustrating all potential cavitation scenarios. As previously explained, these scenarios are explored by maintaining a fixed inlet pressure of p_{in} =20 bar while varying both the opening degree of the inlet reed valve (v_{opn}) and the pumping chamber pressure (p_{cham}). The graph analysis reveals that larger openings of the inlet reed valve result in higher average oil flow velocity near the restricted area. This increased velocity leads to greater pressure drops, which can potentially trigger cavitation.

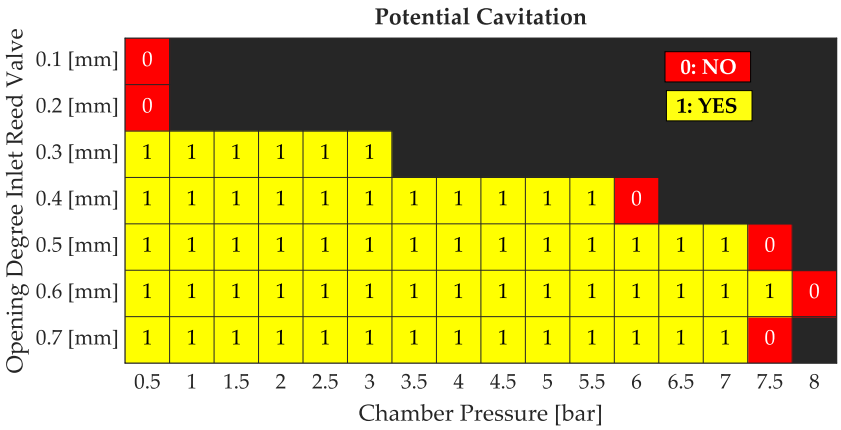

Figure 12 Possible cavitation scenarios considering p_{in} =20 bar and varying v_{opn} from 0.1 mm to 0.7 mm (increments of 0.1 mm) and p_{cham} (increment of 0.5 bar starting from 0,5 bar).

In conclusion, it is important to note that, to validate our CFD analysis, these simulations should also be conducted using the simplified 3D domain rather than a mid-plane section of a slice of this 3D simplified domain in order to better capture the three-dimensional nature of the fluid flow. The mid-plane section (2D domain) was used solely to assess potential cavitation scenarios.

The next step of this research work will be to compare the mean flow rate obtained from experimental tests (over a complete cycle) with the flow rate derived from the mean values of the 3D simplified model, which will be discretized and simulated again using Ansys Fluent. This comparison will account once again for all possible inlet reed valve openings and different pumping chamber pressures to evaluate various steady-state scenarios during the intake stage.

Conclusions

This paper continued an investigation into cavitation potential in a piezohydraulic pump developed at the University of Bath (UK) using the CFD software Ansys Fluent. The simulations were conducted with a fixed inlet pump pressure of p_{in}=20 bar. The study varied the openings of the inlet reed valve (v_{opn}) from 0.1 mm (minimum value) to 0.7 mm (maximum value) in increments of 0.1 mm and examined different values of the pumping chamber pressure (p_{cham}) during the intake stage. Specifically, for each opening degree of the inlet reed valve, the simulations started with a very low pumping chamber pressure (0.5 bar) and increased it by 0.5 bar increments until a specific pumping pressure value no longer induced additional cavitation.

The CFD simulation results showed that as the opening of the inlet reed valve increased and the chamber pressure decreased, both the area of the vapour oil phase and the volume fraction of vapour oil also increased. This trend led to higher occurrences of cavitation due to the higher average oil velocity near the restricted area.

Future investigations will aim to validate the CFD model by comparing its main flow characteristics with experimental data taken from pump testing.

References

[1] E. L. Cavan, E. C. Laurenceau-Cornec, M. Bressac, and P. W. Boyd, "Exploring the ecology of the mesopelagic biological pump," *Prog Oceanogr*, vol. 176, p. 102125, 2019.

[2] E. A. Sideris and H. C. De Lange, "Pumps operated by solid-state electromechanical smart material actuators-A review," *Sens Actuators A Phys*, vol. 307, p. 111915, 2020.

[3] D. J. Laser and J. G. Santiago, "A review of micropumps," *Journal of micromechanics and microengineering*, vol. 14, no. 6, p. R35, 2004.

[4] P. Woias, "Micropumps—past, progress and future prospects," *Sens Actuators B Chem*, vol. 105, no. 1, pp. 28–38, 2005.

[5] N.-C. Tsai and C.-Y. Sue, "Review of MEMS-based drug delivery and dosing systems," *Sens Actuators A Phys*, vol. 134, no. 2, pp. 555–564, 2007.

[6] F. Amirouche, Y. Zhou, and T. Johnson, "Current micropump technologies and their biomedical applications," *Microsystem technologies*, vol. 15, pp. 647–666, 2009.

[7] P. Tamburrano, F. Sciatti, A. R. Plummer, E. Distaso, P. De Palma, and R. Amirante, "A review of novel architectures of servovalves driven by piezoelectric actuators," *Energies (Basel)*, vol. 14, no. 16, p. 4858, 2021.

[8] F. Sciatti, P. Tamburrano, E. Distaso, and R. Amirante, "Digital hydraulic technology: applications, challenges, and future direction," in *Journal of Physics: Conference Series*, IOP Publishing, 2023, p. 012053.

[9] F. Sciatti, P. Tamburrano, E. Distaso, and R. Amirante, "Digital hydraulic valves: Advancements in research," *Heliyon*, 2024.

[10] P. Tamburrano, E. Distaso, A. R. Plummer, F. Sciatti, P. De Palma, and R. Amirante, "Direct drive servovalves actuated by amplified piezo-stacks: Assessment through a detailed numerical analysis," *Actuators*, vol. 10, no. 7, Jul. 2021, doi: 10.3390/act10070156.

[11] P. Tamburrano, P. De Palma, A. R. Plummer, E. Distaso, F. Sciatti, and R. Amirante, "Simulation of a high frequency on/off valve actuated by a piezo-ring stack for digital hydraulics," in *E3S Web of Conferences*, EDP Sciences, 2021, p. 05008.

[12] P. Tamburrano, F. Sciatti, E. Distaso, and R. Amirante, "Comprehensive Numerical Analysis of a Four-Way Two-Position (4/2) High-Frequency Switching Digital Hydraulic Valve Driven by a Ring Stack Actuator," *Energies (Basel)*, vol. 16, no. 21, p. 7355, 2023.

[13] F. Sciatti, P. Tamburrano, P. De Palma, E. Distaso, and R. Amirante, "Detailed simulations of an aircraft fuel system by means of Simulink," in *Journal of Physics: Conference Series*, IOP Publishing, 2022, p. 012033.

[14] P. Tamburrano *et al.*, "Fuels systems and components for future airliners fuelled with liquid hydrogen," in *Journal of Physics: Conference Series*, IOP Publishing, 2022, p. 012041.

[15] F. Sciatti, P. Tamburrano, E. Distaso, and R. Amirante, "Modelling of the Entire Aircraft Fuel System Through Simulink for Accurate Performance Evaluation," in *Fluid Power Systems Technology*, American Society of Mechanical Engineers, 2023, p. V001T01A050.

[16] A. Plummer, D. Adeyemi, N. Sell, F. Sciatti, P. Tamburrano, and R. Amirante, "Fuel System Control for Hydrogen-Powered Aircraft," in *2024 UKACC 14th International Conference on Control (CONTROL)*, IEEE, 2024, pp. 201–202.

[17] P. Tamburrano, F. Sciatti, E. Distaso, L. Di Lorenzo, and R. Amirante, "Validation of a simulink model for simulating the two typical controlled ventilation modes of intensive care units mechanical ventilators," *Applied Sciences*, vol. 12, no. 4, p. 2057, 2022.

[18] H. Li, J. Liu, K. Li, and Y. Liu, "A review of recent studies on piezoelectric pumps and their applications," *Mech Syst Signal Process*, vol. 151, p. 107393, 2021.

[19] J. Kan, K. Tang, Y. Ren, G. Zhu, and P. Li, "Study on a piezohydraulic pump for linear actuators," *Sens Actuators A Phys*, vol. 149, no. 2, pp. 331–339, 2009.

[20] J. Valdovinos and G. P. Carman, "Development of a low-voltage piezohydraulic pump for compact hydraulic systems," *Smart Mater Struct*, vol. 24, no. 12, p. 125008, 2015.

[21] J. Chen, D. Huang, and Z. H. Feng, "A U-shaped piezoelectric resonator for a compact and high-performance pump system," *Smart Mater Struct*, vol. 24, no. 10, p. 105009, 2015.

[22] N. Sell *et al.*, "Design and testing of a high power piezo pump for hydraulic actuation," *J Intell Mater Syst Struct*, 2023.

[23] S. Nayak and R. Muralidhara, "Experimental performance evaluation on piezo-hydraulic pump using flexurally amplified piezoelectric actuators," *Mater Today Proc*, vol. 92, pp. 84–91, 2023.

[24] D. G. Lee, S. W. Or, and G. P. Carman, "Design of a piezoelectric-hydraulic pump with active valves," *J Intell Mater Syst Struct*, vol. 15, no. 2, pp. 107–115, 2004.

[25] P. N. Anh, J.-S. Bae, and J.-H. Hwang, "Computational fluid dynamic analysis of flow rate performance of a small piezoelectric-hydraulic pump," *Applied Sciences*, vol. 11, no. 11, p. 4888, 2021.

[26] J. S. Dong *et al.*, "Design and experimental research on piezoelectric pump with triple vibrators," *Microsystem Technologies*, vol. 23, pp. 3019–3026, 2017.

[27] T. Peng *et al.*, "A high-flow, self-filling piezoelectric pump driven by hybrid connected multiple chambers with umbrella-shaped valves," *Sens Actuators B Chem*, vol. 301, p. 126961, 2019.

[28] N. Sell, F. Sciatti, A. Plummer, and T. Love, "Design and testing of a multi-cylinder piezo pump for hydraulic actuation," *Energies (Basel)*, 2024.

[29] B. Pečar, D. Križaj, D. Vrtačnik, D. Resnik, T. Dolžan, and M. Možek, "Piezoelectric peristaltic micropump with a single actuator," *Journal of Micromechanics and Microengineering*, vol. 24, no. 10, p. 105010, 2014.

[30] N. Sell, A. Plummer, N. Johnston, and J. du Bois, "Simulating a high frequency piezo pump with disc reed valves," in *Scandinavian International Conference on Fluid Power*, 2021, pp. 274–282.

[31] S. N. Muralidhara and R. Rao, "Design and simulation of high pressure piezohydraulic pump with active valves," in *2016 International Conference on Electrical, Electronics, and Optimization Techniques (ICEEOT)*, IEEE, 2016, pp. 1608–1613.

[32] J. Zhang, Q. Xia, D. Lai, O. Akiyoshi, and Z. Hong, "Discovery and analysis on cavitation in piezoelectric pumps.," *Chinese Journal of Mechanical Engineering(English Edition)*, vol. 17, no. 4, pp. 591–594, 2004.

[33] K. Opitz, O. Schade, and E. Schlücker, "Cavitation in reciprocating positive displacement pumps," in *Proceedings of the 27th international pump users symposium*, Turbomachinery Laboratory, Texas A&M University, 2011.

[34] Y. Ye, J. Chen, Q. S. Pan, and Z. H. Feng, "Suppressing the generation of cavitation by increasing the number of inlet check valves in piezoelectric pumps," *Sens Actuators A Phys*, vol. 293, pp. 56–61, 2019.

[35] X. He, X. Deng, S. Yang, Y. Bi, and Q. Jiang, "Numerical analysis of cavitation flow in vortex-valve piezoelectric micropump," *Drain. Irrig. Mach*, vol. 27, pp. 352–356, 2009.

[36] B. Pečar *et al.*, "Micropump operation at various driving signals: numerical simulation and experimental verification," *Microsystem Technologies*, vol. 21, pp. 1379–1384, 2015.

[37] T. Dolžan, B. Pečar, M. Možek, D. Resnik, and D. Vrtačnik, "Self-priming bubble tolerant microcylinder pump," *Sens Actuators A Phys*, vol. 233, pp. 548–556, 2015.

[38] F. Sciatti *et al.*, "Numerical Analysis of a High-Power Piezoelectric Pump using Computational Fluid Dynamics (CFD) Simulations," Springer, Ed., 2024.

[39] "https://www.piceramic.com/en/products/piezoceramic-actuators/stack-actuators/p-010xxh-p-025xxh-pica-thru-ring-actuators-102800," Accessed on June 2024.

[40] A. Loseille, "Unstructured mesh generation and adaptation," in *Handbook of Numerical Analysis*, vol. 18, Elsevier, 2017, pp. 263–302.

[41] M. Nezamirad, A. Yazdi, S. Amirahmadian, N. Sabetpour, and A. Hamedi, "Utilization of Schnerr-Sauer cavitation model for simulation of cavitation inception and super cavitation," *International Journal of Aerospace and Mechanical Engineering*, vol. 16, no. 3, pp. 31–35, 2022.

[42] E. Pal, I. Kumar, J. B. Joshi, and N. K. Maheshwari, "CFD simulations of shell-side flow in a shell-and-tube type heat exchanger with and without baffles," *Chem Eng Sci*, vol. 143, pp. 314–340, 2016.

[43] J. Xiao *et al.*, "Assessment of different CFD modeling and solving approaches for a supersonic steam ejector simulation," *Atmosphere (Basel)*, vol. 13, no. 1, p. 144, 2022.